

Synthesis of $\text{La}_{2-x}\text{Sr}_x\text{CuO}_4$ films via atomic-layer-by-layer molecular-beam epitaxy

X. Xu, I. Bozovic

To be published in "APL Materials"

June 2022

Condensed Matter Physics and Materials Science Department
Brookhaven National Laboratory

U.S. Department of Energy

USDOE Office of Science (SC), Basic Energy Sciences (BES) (SC-22)

Notice: This manuscript has been authored by employees of Brookhaven Science Associates, LLC under Contract No. DE-SC0012704 with the U.S. Department of Energy. The publisher by accepting the manuscript for publication acknowledges that the United States Government retains a non-exclusive, paid-up, irrevocable, world-wide license to publish or reproduce the published form of this manuscript, or allow others to do so, for United States Government purposes.

DISCLAIMER

This report was prepared as an account of work sponsored by an agency of the United States Government. Neither the United States Government nor any agency thereof, nor any of their employees, nor any of their contractors, subcontractors, or their employees, makes any warranty, express or implied, or assumes any legal liability or responsibility for the accuracy, completeness, or any third party's use or the results of such use of any information, apparatus, product, or process disclosed, or represents that its use would not infringe privately owned rights. Reference herein to any specific commercial product, process, or service by trade name, trademark, manufacturer, or otherwise, does not necessarily constitute or imply its endorsement, recommendation, or favoring by the United States Government or any agency thereof or its contractors or subcontractors. The views and opinions of authors expressed herein do not necessarily state or reflect those of the United States Government or any agency thereof.

Synthesis of $\text{La}_{2-x}\text{Sr}_x\text{CuO}_4$ films via atomic-layer-by-layer molecular-beam epitaxy

Xiaotao Xu^{1,2}, Xi He^{1,3,4}, Xiaoyan Shi² and Ivan Božović^{1,3,4}

- ¹ Condensed Matter Physics and Materials Science Department, Brookhaven National Laboratory, Upton, New York 11973-5000, USA
² Department of Physics, The University of Texas at Dallas, Richardson TX 75080-3021, USA
³ Department of Chemistry, Yale University, New Haven CT 06520, USA
⁴ Energy Science Institute, Yale University, West Haven CT 06516, USA

ABSTRACT

Atomic layer-by-layer molecular beam epitaxy (ALL-MBE) is a sophisticated technique to synthesize high-temperature superconductor (HTS) materials. ALL-MBE produces single-crystal HTS films with atomically smooth surfaces and interfaces, as well as precise multilayer heterostructures engineered down to a single atomic layer level. This enables the fabrication of tunnel junctions, nanowires, nanorings, and other HTS devices of interest. Our group has been focused on ALL-MBE synthesis and materials science of $\text{La}_{2-x}\text{Sr}_x\text{CuO}_4$ (LSCO), a representative HTS cuprate. In the past two decades, we have synthesized over three thousand LSCO thin films and characterized them by a range of analytical techniques. Here, we present in full detail a systematic process for the synthesis and engineering of atomically perfect LSCO films. The procedure includes the preparation of substrates, calibration of the elemental sources, the recipe for ALL growth of LSCO films without any secondary-phase precipitates, post-growth annealing of the films, and ex-situ film characterization. This report should aid replication and dissemination of this

This is the author's peer reviewed, accepted manuscript. However, the online version of record will be different from this version once it has been copyedited and typeset.
PLEASE CITE THIS ARTICLE AS DOI:10.1063/1.50087223

technique of synthesizing single-crystal LSCO films, for basic research as well as for HTS electronics applications.

I. BACKGROUND AND MOTIVATION

The discovery of high-temperature superconductivity (HTS) in $\text{La}_{2-x}\text{Ba}_x\text{CuO}_4$, 35 years ago [1], has triggered extensive basic-physics research aimed at clarifying the underlying mechanism. [2-21] In parallel, the materials science of copper oxides have been studied in great detail, to develop HTS tapes and wires for high-power applications as well as thin films and heterostructures for HTS-based electronics. One of the most advanced techniques to synthesize HTS cuprates is atomic layer-by-layer molecular beam epitaxy (ALL-MBE). [22,23] It produces atomically perfect thin films with one-monolayer (ML) resolution. Precise surface and interface control make it particularly useful for device fabrication such as interface superconductors, trilayer (“sandwich”) Josephson junctions, and artificial superlattices.

The Oxide-MBE group at Brookhaven National Lab has been focused on studying HTS physics and materials science for the past two decades. In what follows we describe the synthesis method that we have developed for the $\text{La}_{2-x}\text{Sr}_x\text{CuO}_4$ (LSCO), an archetype HTS cuprate. Both La and Sr are amenable to well-controlled thermal evaporation, making LSCO a suitable candidate for ALL-MBE synthesis. [24-27] The “parent” compound LCO (La_2CuO_4) features a single perovskite-like copper-oxygen plane sandwiched between two lanthanum-oxygen charge-reservoir planes. By substituting a certain fraction x (the “doping level”) of lanthanum atoms with strontium atoms, one can dope LCO from an antiferromagnetic insulator to a non-superconducting metal. Superconductivity emerges at $x_{min} \approx 0.06$, reaches the maximum $T_c \approx 42$ K at $x_{opt} = 0.16$, and vanishes at $x_{max} \approx$

0.26. We synthesize LSCO films with any desired x , which can even be varied at will within each ML, using an ALL-MBE system that was specifically designed for the growth of copper oxides. [23]

In what follows, we present the details of a systematic procedure for synthesis and engineering of atomically perfect LSCO films, including substrate preparation, source calibration, ALL growth of LSCO films, post-growth annealing, and ex-situ film characterization. We hope that this will be of value to others interested in synthesizing single-crystal LSCO films, for basic research as well as for HTS electronics applications.

II. SUBSTRATE PREPARATION AND CHARACTERIZATION

Single-crystal LaSrAlO_4 (LSAO) and SrTiO_3 (STO) are commonly used as substrates for LSCO growth. The lattice constant of the optimally doped LSCO ($x = 0.16$) is $a_0 = 3.777 \text{ \AA}$. The lattice constant of LSAO is 0.5% shorter ($a = 3.755 \text{ \AA}$), while in STO it is 3% longer ($a = 3.905 \text{ \AA}$) than in LSCO. Since the substrate serves as a template for the epitaxial film, the quality of the substrate is essential for successful ALL-MBE synthesis. We have adopted the following preparation methods for LSAO and STO substrates, respectively.

A. LSAO preparation and characterization

Our standard LSAO substrates are $10 \times 10 \times 1 \text{ mm}^3$ in size; one side is epi-polished perpendicular to the [001] crystallographic direction, while the other side is deliberately left rough (sand-polished) to improve the sticking of the backside coating (described in section 3 below). In recent years, most of these substrates we purchased from MTI Corporation. We process LSAO substrates as follows.

First, an LSAO substrate is cleaned in the ultrasonic tank in de-ionized water (resistivity $> 18 \text{ M}\Omega\text{cm}$) for 30 seconds. Next, it is rinsed with ethyl alcohol and dried with nitrogen gas. The substrate is then

placed face-up in a custom-built sapphire crucible together with a slightly larger ($13 \times 13 \times 0.5 \text{ mm}^3$) LaAlO_3 (LAO) substrate that is placed closely above it (0.3 mm gap); the schematic of this assembly is shown in Fig 1. The whole setup is annealed in a tube furnace at $950 \text{ }^\circ\text{C}$ in the air for 1 h. The role of the LAO substrate here is to provide a cation-rich environment that compensates for evaporation (of Al, largely) from LSAO and suppresses the formation of SrO precipitates on the LSAO surface. [28]

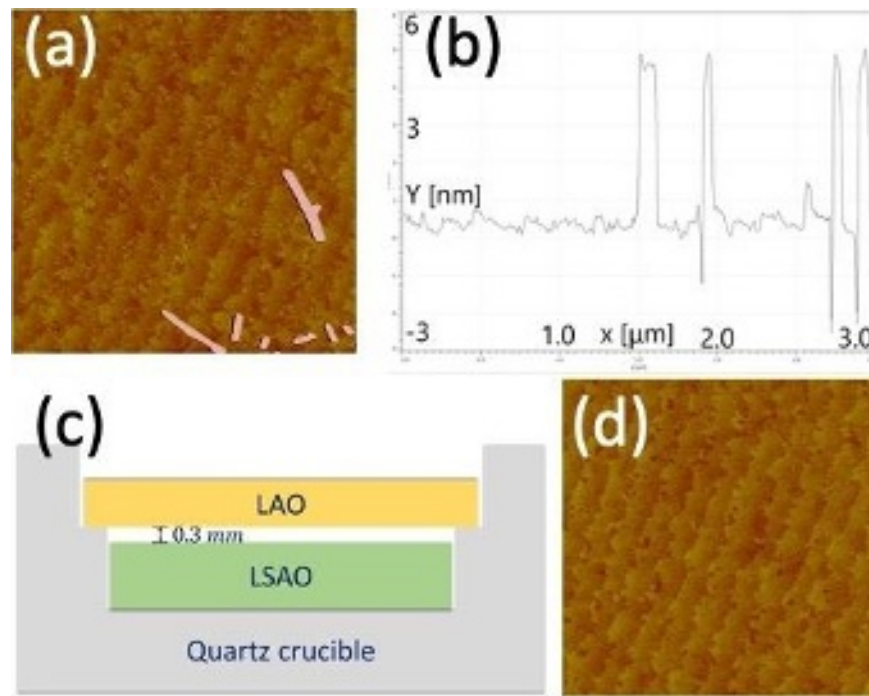


Figure 1: LSAO substrate annealing. **a**, Atomic force microscopy (AFM) image of an as-received LSAO substrate; the field of view is $3 \times 3 \mu\text{m}^2$. Large particulates are seen on the surface. **b**, The AFM height profile along the red line in **a**. The defects are about 5 nm tall. **c**, A schematic of the setup for LSAO annealing. **d**, An AFM image of the same substrate after the annealing process; the rms roughness is 0.17 nm, so the surface is essentially atomically flat.

B. STO preparation and characterization

The typical STO substrates that we use are also $10 \times 10 \times 1 \text{ mm}^3$, one-side epi-polished perpendicular to the [001] direction, the other side sand-polished, and come from MTI Corporation. To prepare a clean, single- (TiO_2) termination surface, STO substrate can be treated with buffered hydrofluoric acid. [29,30] However, given the safety hazards involved, we have instead adopted the following acid-free two-stage STO cleaning and annealing procedure. [31]

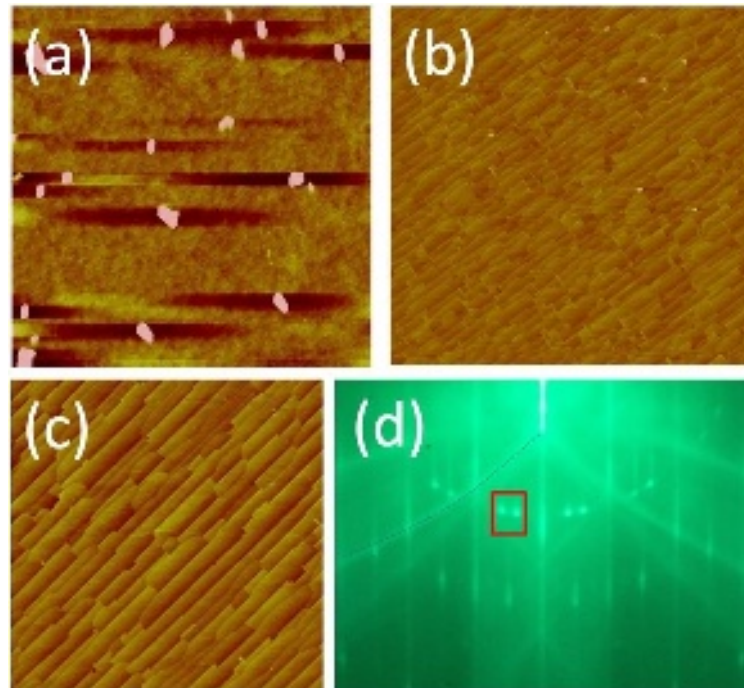


Figure 2: STO substrate annealing. **a**, AFM image of an as-received STO substrate; the field of view is $3 \times 3 \mu\text{m}^2$. The surface shows an abundance of large precipitates. **b**, Substrate surface after 1st annealing process. Tiny white dots are SrO out-diffusions. **c**, Substrate surface after 2nd annealing process. Rms roughness is 0.25 nm. **d**, RHEED image of the same substrate after 2nd annealing. The Blue dashed line is a Kikuchi line. The red box highlights a RHEED feature characteristic of TiO_2 -terminated surface.

An AFM image of an as-received STO substrate is shown in Fig 2. The substrate is first cleaned with de-ionized water in an ultrasonic bath for 30 seconds and then annealed in air at $1,000^\circ\text{C}$ for 1 hour. It is then sonicated again for 30 seconds and annealed in air at $1,100^\circ\text{C}$ for another hour.

After the first annealing, the AFM image of the STO substrate shows a terraced surface, with the step width in the 100~200 nm range. SrO precipitates that presumably originate from out-diffusion can be seen at the step edges. However, after the second sonication + annealing cycle, these SrO particulates are effectively removed. Terraces become smoother and wider (200~300 nm) as well. Subsequent inspection of the substrate surface by Reflection high-energy electron diffraction (RHEED) indicates that it is terminated by TiO₂.

C. Backside coating with SrRuO₃

To better absorb the radiation from a quartz-lamp heater during the film deposition, the backside of the substrate is coated with SrRuO₃ (SRO) using magnetron sputtering. SRO was chosen because of its superior thermal and chemical stability and undetectably small vapor pressure when exposed to a high temperature and ozone atmosphere, which we need for epitaxial growth of LSCO. During SRO sputtering, the substrates are held at 650°C under a mixed-gas environment (100 mTorr partial pressure of Ar and 33 mTorr of O₂). The radio-frequency power for sputtering is set at 30 W for 4 days and then elevated to 40 W for another 4 days. We intentionally use a low deposition rate since this helps to alleviate the peeling of the backside coating from the substrate once it is heated up in the ALL-MBE chamber.

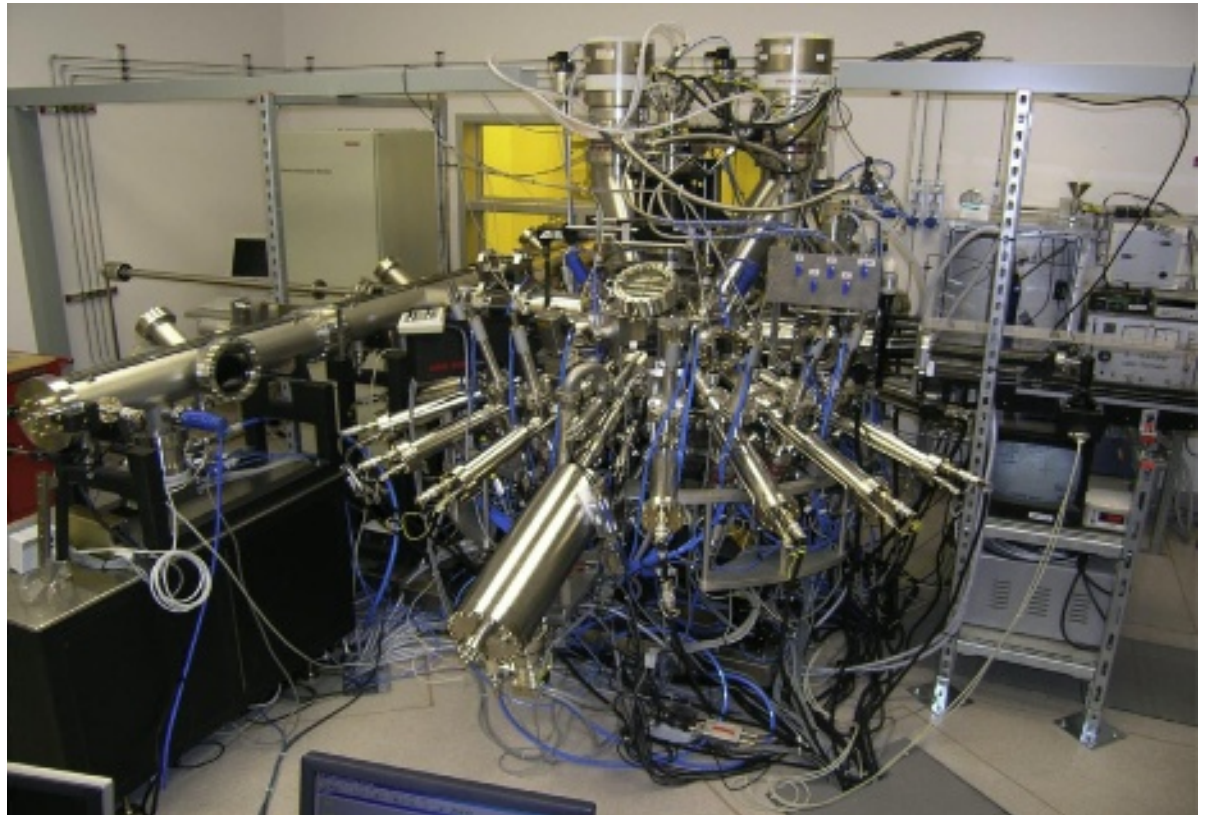
We would also like to mention that in recent years more advanced methods have been developed for the treatment of oxide substrates. In particular, Jochen Mannhart's group at the Max Planck Institute has demonstrated that excellent substrate surfaces can be prepared by in-situ annealing using a laser heater. [32,33] The oxide substrates of interest have high absorption at the CO₂ laser wavelength, and therefore no backside coating is required. Several other groups have been using laser heaters with success. With this motivation, we are also in the process of adding a laser heater to our ALL-

MBE system, and we plan to explore this method of preparation of substrate surfaces in our future experiments.

III. ALL-MBE TECHNIQUE – GENERAL FEATURES

A. MBE system description

The atomic-layer-by-layer molecular beam epitaxy (ALL-MBE) system at Brookhaven National Laboratory is a custom multi-chamber ultra-high vacuum (UHV) apparatus specifically designed for the synthesis of superconducting oxides (Fig. 3). It is equipped with 16 metal sources (either Knudsen cells or rod-fed electron beam sources) and a pure ozone source. Several surface analytical tools are integrated *in situ*, including a double-deflection RHEED system and a time-of-flight ion-scattering-and-recoil spectroscopy (TOF-ISARS) system. [23]



This is the author's peer reviewed, accepted manuscript. However, the online version of record will be different from this version once it has been copyedited and typeset.
PLEASE CITE THIS ARTICLE AS DOI:10.1063/1.5008723

Figure 3. ALL-MBE system at BNL. The MBE synthesis chamber features 16 thermal evaporation sources, a pure ozone source, RHEED, TOF-ISARS, scanning QCM, etc. The 20-foot long transfer chamber enables the sample to be transported under ultra-high vacuum to a processing chamber in the adjacent clean room, for lithography, and back again for the second synthesis process step, if needed.

B. Ozone system

The ALL-MBE system is also equipped with a home-built ozone distillation system that supplies pure ozone gas into the chamber during the growth. A schematic is shown in Fig. 4. After being generated from O_2 gas by arc discharge, ozone is liquefied, purified, and stored in the ozone condenser vessel cooled by liquid nitrogen. A water-cooled stainless-steel tube, reaching within a few centimeters from the substrate, is used to introduce ozone gas into the ALL-MBE chamber. Ozone partial pressure during the growth is controlled by a proportional integral derivative (PID) program.

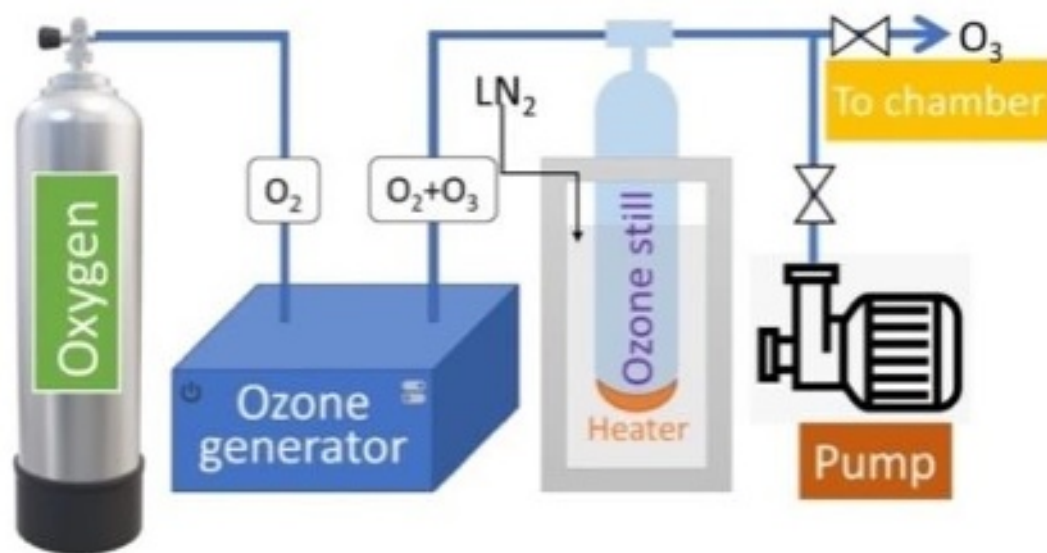


Figure 4: Schematics of the ozone distillation setup. Ultrahigh purity oxygen gas is supplied to a commercial arc-discharge ozone generator. The $O_2 + O_3$ mixture is condensed in the quartz vessel cooled with liquid nitrogen. Then, the liquid is warmed up so that O_2 evaporates and is pumped out, leaving a pure O_3 liquid. Ozone vapor is then supplied to the MBE growth chamber.

C. Substrate monitoring

A digital camera is used for monitoring the substrate and positioning of the quartz-crystal monitor (QCM). The temperature of the substrate surface is measured using a two-wavelength high-temperature infrared pyrometer with a video-aiming function. The pyrometer measures the temperature at the focal spot of 3 mm diameter on the substrate, to the accuracy of 0.1°C.

D. Source calibration

To synthesize LSCO, we use 6 Knudsen cells, two each for La, Sr, and Cu. Since the sources are not perpendicular to the substrate, this generates a (small, 4% from one side to another) gradient in the deposition rate across the substrate. To compensate for this, for each element we use a pair of sources that are positioned across one another, on the opposite sides of the circle; this provides a uniform deposition rate over the substrate area. The absolute deposition rate of each Knudsen cell is measured before film deposition by QCM to the accuracy of 0.0001 atomic layers (AL) per second. During the calibration ozone is delivered into the chamber and maintained at the same partial pressure as it is during the actual film growth, to ensure that the chamber environment remains the same.

Given that the atomic fluxes provided by effusion cells stay stable for hours with a drift of a few percent or less, we perform source calibration routinely before each film growth. On occasion, this procedure is repeated after the growth, as well, as an additional check. For the best growth-to-growth reproducibility, we try to keep the deposition rates for each element constant, as follows: the La_2O_3 and CuO rates are kept at 0.010 AL/sec, and the SrO rate at 0.005 AL/sec.

IV. SYNTHESIS OF LSCO FILMS ON LSAO SUBSTRATES

A. Overdoped LSCO buffer layer

We always start the synthesis of LSCO films by first depositing one or two MLs of highly overdoped LSCO ($x = 0.40$) as a buffer layer, before the growth of other LSCO compositions. The function of this buffer layer is to “absorb” the lattice (crystallographic) and electrostatic (“polarization catastrophe”) mismatch between the substrate and subsequent LSCO film, offering a more favorable starting point for epitaxy of the desired LSCO phase. [34-36]

B. LSCO film growth on LSAO substrates

LSCO has an intrinsically layered structure: one ML, about 0.66 nm thick, consists of two (La, Sr)-O layers and one CuO₂ layer. (One unit cell contains two MLs, displaced horizontally by one-half the unit cell diagonal, so $c_0 \approx 1.32$ nm.) The atomic layer-by-layer growth mode is realized by shuttering the sources; pneumatic shutters are computer-controlled so that the exact number of La, Sr, and Cu atoms is deposited to the surface of the growing film in the desired sequence. Typically, we keep the substrate at ~ 630 °C, under the background ozone partial pressure of 1.0×10^{-5} Torr. We start the growth of one ML of LSCO by depositing two (La,Sr)-O planes, with the precise pre-selected ratio of La and Sr atoms. After both La and Sr shutters are closed, we wait for 30 seconds to allow the atoms on the surface to relax towards their equilibrium positions. Then we open the two Cu shutters to deposit one CuO₂ layer. The growth of each ML takes about three minutes. Single-phase LSCO is synthesized by repeating sequential deposition of (La, Sr)-O and CuO₂ layers. Under ALL deposition, the film thickness can be controlled digitally, down to a single ML. Moreover, at the end of one period, one can switch to another composition at will, providing much flexibility to fabricate artificial structures such as multilayer junctions and superlattices.

C. RHEED monitoring

In-situ RHEED provides crystallographic information about the film surface during growth, in real-time. [37] Few typical RHEED images are shown in Fig. 5. For an LSAO substrate (Fig. 5a), the most prominent features are the 5 main streaks, originating from the (0,-2), (0,-1), (0,0), (0,1) and (0,2) Bragg diffraction rods. The separation of these streaks in k -space is proportional to the inverse of the in-plane lattice constant of LSAO, $a_0 = 0.38$ nm. Similar principal streaks are also seen in LSCO films (Figs. 5b, c, and d), with the same spacing as in the LSAO substrate; these films are thin and pseudo-morphic with the substrate, i.e., they have the same in-plane lattice constant $a_0 = 0.38$ nm as LSAO.

A new feature characteristic of LSCO films, and absent in LSAO, are multiple satellite streaks ('sidebands') surrounding the principal streaks. Such sidebands feature prominently in the growth of LSCO films within the entire doping range. The number of sidebands N characterizes the superstructure modulation of the surface, with the supercell period $N \times a_0$ in real space. The detailed atomistic understanding of this surface reconstruction is still missing as of the time of writing of this paper.

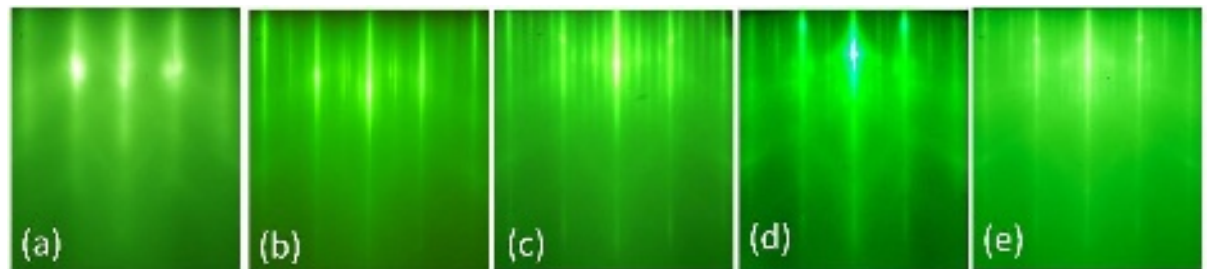


Figure 5. RHEED patterns. (a) LSAO substrate. (b) Underdoped LSCO($x = 0.14$) film. (c) Optimally doped LSCO($x = 0.16$) film. (d) overdoped LSCO($x = 0.24$) film. (e) Heavily overdoped LSCO($x = 0.30$) film.

Other prominent features in Fig. 5c are the very bright specular spot, the long and sharp streaks, visible diagonal (“Kikuchi”) lines, and Laüe-circle reflections. All these features are indications of an atomically flat surface and high crystallinity of the film.

The intensity of the specular RHEED reflection shows periodic oscillations in time (Fig. 6), as the surface morphology changes from complete coverage (smooth surface, strong specular reflection) to a partial coverage with some islands (rough surface, weaker specular and stronger diffuse reflection) and back to complete coverage. [37] These RHEED oscillations are another qualitative indicator of the growth dynamics. One oscillation period corresponds to the growth of one ML of LSCO. The fact that the peak intensity did not decay with time illustrates that the film surface remained equally flat and smooth for many layers.

LSAO substrates we use are typically cut orthogonal to the *c*-axis, i.e., the crystallographic [001] direction. By rotating the substrate, the shallow-angle incident electron beam is brought to be almost parallel to the crystallographic [100] direction. So, we can infer from the RHEED patterns that the Cu-O-Cu bonds are parallel to the Al-O-Al bonds in the substrate, i.e., the crystallographic [100] direction in LSCO coincides with that in LSAO.

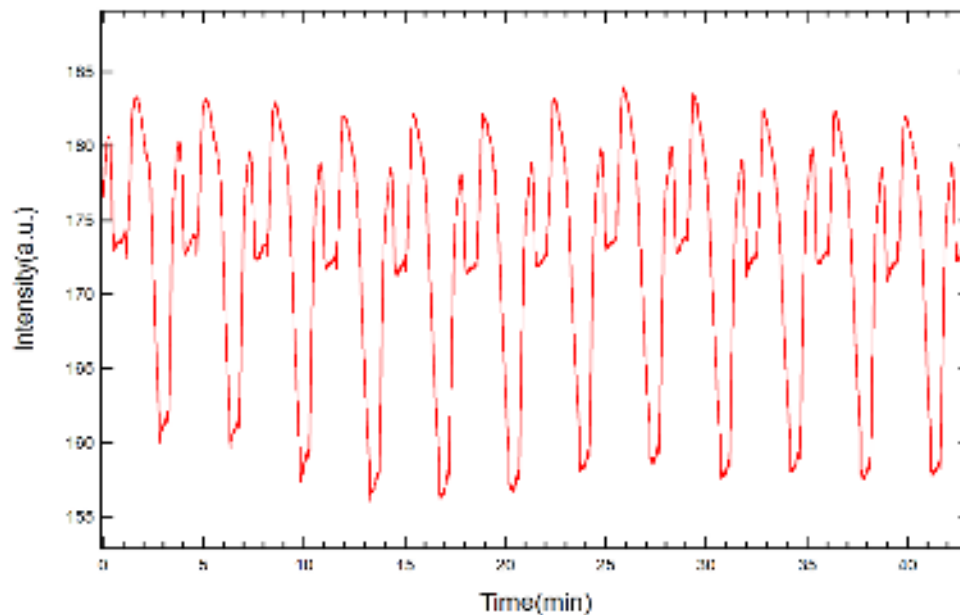


Figure 6. Oscillations of the intensity of specular RHEED spot

D. RHEED dynamics as a diagnostic tool for fine-tuning the stoichiometry

In general, maintaining the correct stoichiometry is one of the most difficult aspects of growing films of cuprates or other complex oxides, by any technique. On occasion, secondary-phase precipitates form in the film, e.g., due to an error in stoichiometry. [38] These may be detectable from RHEED images, since they give rise to transmission spots at Bragg diffraction angles, at the position characteristic of that (unwanted) phase – e.g., La_2O_3 , SrO or CuO , in the case of LSCO film growth. The advantage of MBE and RHEED is that one can detect such precipitates while they are still very small, on the 10-20 nm scale, as these produce large (due to Scherrer broadening) “blobs” in the RHEED pattern. Then, in some favorable cases, one may be able to make a correction in the stoichiometry and dissolve or cover such defects. [37] However, when the secondary phase (e.g., CuO) is thermodynamically more stable than the targeted cuprate compound (e.g., LSCO), then once the precipitates are nucleated they keep growing like cancer and contaminate the film. Once we observe these precipitate blobs in RHEED, it is too late — the film will not be single-phase. This in

turn modifies the film properties, including superconductivity, and when studying such a film one indeed may be deceived by extrinsic effects.

By studying the RHEED pattern evolution, we have developed a novel diagnostic strategy based on the real-time dynamics of RHEED features, enabling us to fine-tune and correct the stoichiometry of LSCO films before the formation of any secondary-phase precipitates. Take, for example, the synthesis of optimally doped LSCO. During the deposition of the CuO layer, the superstructure modulation of the surface appears with four sidebands, which become long and sharp (Fig 7a). When the Cu shutters are closed, the intensity of the sidebands reaches the maximum. During the deposition of the subsequent (La,Sr)O layer, these four sidebands gradually vanish, and instead, a new pattern appears, with two or three sidebands (Fig. 7b). During the deposition of the next CuO layer, after some time the four sidebands appear again, etc.

Our tactics to prevent nucleation of the secondary phases rely on timing the appearance of the 4 sidebands during the CuO layer deposition. More specifically, we measure the time interval from the moment when the pattern typical of a (La,Sr)O layer is replaced by the 4-streak pattern of the CuO₂ layer. We have found empirically that, given our deposition rates of 0.010 AL/sec for Cu and La, the optimal “clean CuO₂ time interval” is around 10-15 seconds. Note that the duration of this clean-CuO₂ time is a very sensitive function of the deposition (shuttering) times. If we change the growth “recipe” by changing the Cu shuttering time by just a couple of percent, this raises or lowers the clean-CuO₂ time significantly (by a few seconds) in the following one or two LSCO layers.

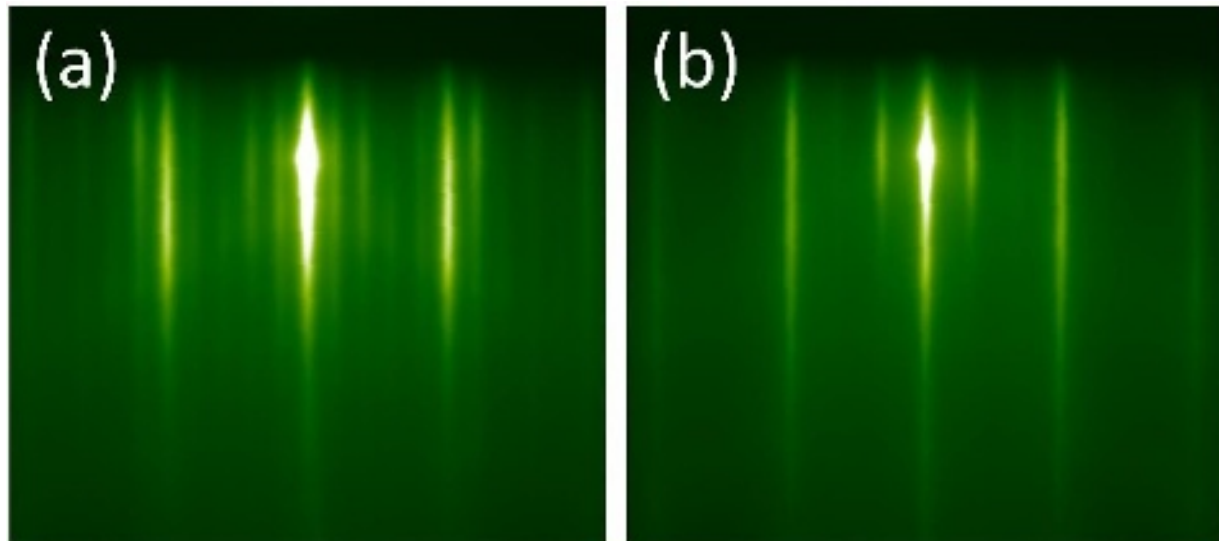


Figure 7. RHEED patterns of an optimally doped LSCO film. a, After the CuO_2 layer. **b,** after the $(\text{La,Sr})\text{O}$ layer.

By repeated and systematic experimentation, we have established the following causal relation. If the clean- CuO_2 time falls outside the 10-15 seconds range, by itself (i.e., because of the error in the absolute rate calibration, the drift in the atomic flux due to a thermal fluctuation of the Knudsen cell, because the source material is depleted, etc.) or by the action of the film grower (e.g. a change in the growth recipe, which changes the shuttering times), nucleation of secondary-phase precipitates can be detected by RHEED within a few subsequent LSCO layers. Cu deficiency causes a shorter clean- CuO_2 time, which leads to the formation of La_2O_3 defects. Excess Cu atoms, on the other hand, result in a longer clean- CuO_2 time, and CuO defects appear subsequently. To prevent that, we manually intervene in the film growth receipt by increasing or decreasing the Cu shuttering time and hence the number of Cu atoms deposited on the surface in one shuttering cycle, and adjust it so that we keep the clean- CuO_2 time within the 10-15 second window. This protocol ensures the synthesis of LSCO films without any secondary-phase precipitates.

E. Adjusting the oxygen stoichiometry

Another critical issue in the synthesis of LSCO films is achieving the desired oxygen content. While commonly referred to as the “214” structure, the actual chemical composition is $\text{La}_{2-x}\text{Sr}_x\text{CuO}_{4+\delta}$, where δ can be positive, zero, or negative. Undoped LCO and underdoped LSCO are amenable to intercalation of extra oxygen (i.e., $\delta > 0$), which occupies sites interstitial between the two (La,Sr)O layers. When LSCO films are grown on LSAO, they are under compressive strain, so the unit cell contracts in-plane while expanding out-of-plane. This, in turn, facilitates the incorporation of interstitial oxygen. [39] On the other hand, overdoped LSCO is prone to the formation of oxygen vacancies (so, $\delta < 0$), the concentration of which increases nonlinearly with overdoping. [40] The driving force for this is chemistry — it is very hard to oxidize copper to more than the (+2)-state, while oxygen favors the closed-shell $2s^2p^6$ configuration (the O^{2-} ionic state). As the result, some oxygen is not incorporated during the deposition of Cu, which results in the formation of defective $\text{CuO}_{2-\delta}$ layers. These oxygen vacancies are detrimental to both normal conductivity (they increase the residual resistivity) and superconductivity (they decrease T_c and the superfluid density). [41]

In theory, one could solve this problem by controlling and maintaining the ideal $\delta = 0$ oxygen stoichiometry just by adjusting the oxidation power — lowering it for underdoped and increasing it for overdoped LSCO. The oxidation power can be controlled by adjusting the substrate temperature T and the ozone partial pressure p . In the $\log(p)$ - $1/T$ plots, the equal-oxidation power contours are straight lines. [42] In practice, to stay within the MBE growth regime, which requires a high vacuum, while still keeping sufficient oxidation power to form the 214 structure, we are limited to operating within a relatively narrow (T, p) parameter range during the ALL-MBE synthesis.

However, once the film is grown, we can increase the ozone pressure and post-anneal the films *in situ*, after we protect all hot filaments (i.e., after we valve off all the Knudsen-cell sources and switch off the analytical tools such as RHEED and the residual gas analyzer). Annealing at a high temperature improves the film crystallinity and makes the superconducting transition sharper. Given the exponential character of the p - T dependence, annealing at a temperature lower than the growth temperature under high partial pressure of ozone can dramatically increase the oxidation power, filling the oxygen vacancies. On the other hand, annealing in a vacuum at a well-chosen lower temperature can extricate the interstitial oxygen atoms without removing the ‘structural’ oxygen that is inherent to the 214 crystal structure.

To find the optimal procedure, we have extensively studied the post-annealing of LSCO films over a broad range of (T, p) conditions. In the last two decades, we synthesized over 3,000 LSCO films, characterizing them before and after post-annealing *in situ* or *ex-situ*. Here are some recipes for multi-step *in situ* post-annealing. We anneal underdoped LSCO films under the 10^{-4} Torr partial pressure of ozone at 675°C for 5 minutes, then under the same pressure at 610°C for 30 minutes, then in a high vacuum at about 250°C for 30 mins, and then cool them in vacuum to the room temperature. Optimally doped LSCO films are heated up to 675°C for 5 minutes, then cooled to 610°C for 30 minutes, then cooled down to room temperature, under the 10^{-4} Torr partial pressure throughout. Overdoped LSCO films are annealed under the 10^{-4} Torr partial pressure at 600°C for up to 4 hours and then cooled down under the same ozone environment to the room temperature.

V. LSCO FILM CHARACTERIZATION

The first crystallographic and morphological information about our films we obtain in real-time, using *in-situ* RHEED. After the growth, we characterize every film *ex-situ* by Atomic force

microscopy (AFM) and by Mutual inductance (MI) measurements. [43] We also frequently deposit gold contact pads on selected films and measure the temperature dependence of resistivity. We pattern some film into multiple Hall bar devices and measure the temperature dependence of the Hall effect and magnetoresistance. Selected films are studied by X-ray diffraction (XRD), in-house, or by our collaborators that use synchrotron radiation for the highest resolution, by Transmission electron microscopy (TEM), THz spectroscopy, Resonant inelastic X-ray scattering (RIXS), ultrafast pump-probe spectroscopy, shot-noise measurements, and much more. Altogether, these experiments provide a huge database that contains a great wealth of information on HTS cuprates. Here, we just briefly describe the two characterization techniques, AFM and MI, that we routinely apply to every film we synthesize. In just a few hours, the AFM and MI measurements can be completed, providing a contactless and quick characterization most relevant for superconducting thin film research. Contactless operation offers protection against contamination and modification of the sample surface.

A. Atomic force microscopy

Fig. 8 displays an AFM image typical of good LSCO film synthesized by ALL-MBE on an LSAO substrate. Due to an inevitable slight miscut (typically $0.1^\circ - 0.5^\circ$) of the substrate away from the ideal crystallographic plane perpendicular to the [001] direction, the substrate surface shows terraces separated by one-ML-tall steps. Under ALL growth, these steps and terraces are projected onto the film surface, as well. The overall final rms surface roughness of the film is 0.443 nm, which is less than the height of one ML (0.66 nm), so the terraces are essentially atomically flat.

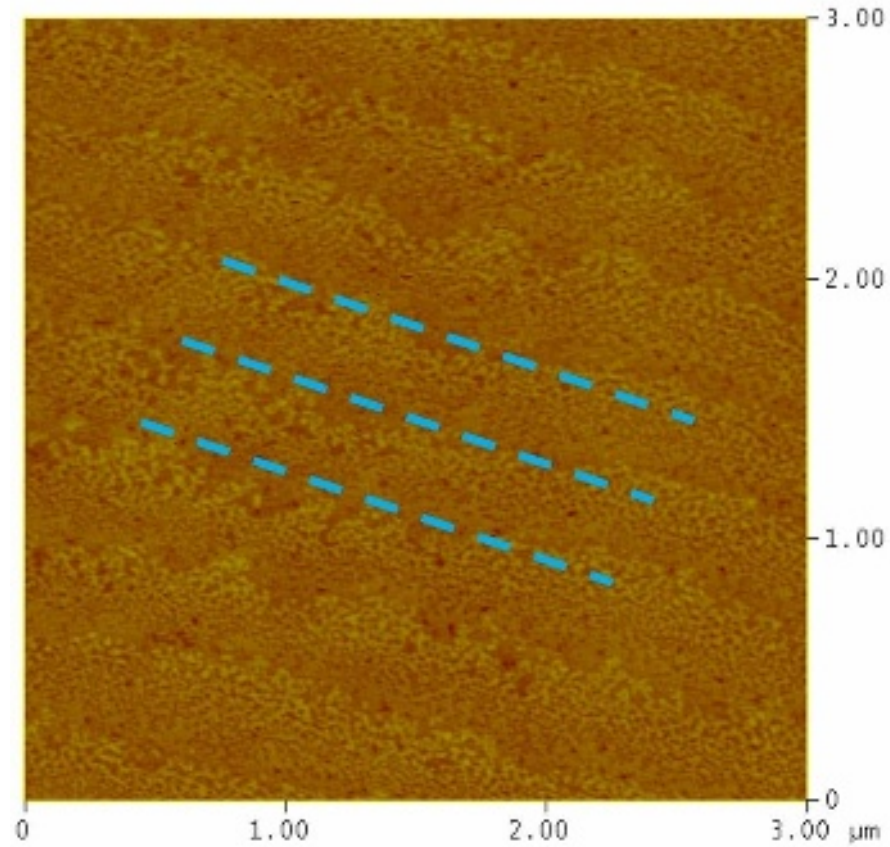


Figure 8: An AFM image of an LSCO film. The field of view is $3 \times 3 \mu\text{m}^2$. Terrace steps, marked with blue lines, originate from a slight miscut of the substrate away from the ideal plane perpendicular to the crystallographic [001] direction. The rms surface roughness is 0.17 nm.

B. Mutual inductance

The principle of the MI experiment is very simple. A film is placed between a drive coil and a pickup coil. The drive coil is ac driven (in the kHz frequency range) and it generates a magnetic field that induces AC in the pick-up coil. The real part of emf in the pickup coil is proportional to the mutual inductance, and it shows diamagnetic screening (the Meissner effect) when the film becomes superconducting. The imaginary part is proportional to the AC conductivity and it shows a sharp peak near T_c . If the geometry of the coils and films, as well as the electronic, mechanic, and thermal aspects of the setup, are all tightly controlled, the penetration depth λ and the ac conductivity can be derived from the complex impedance with remarkable absolute accuracy (better than 1%). [43]

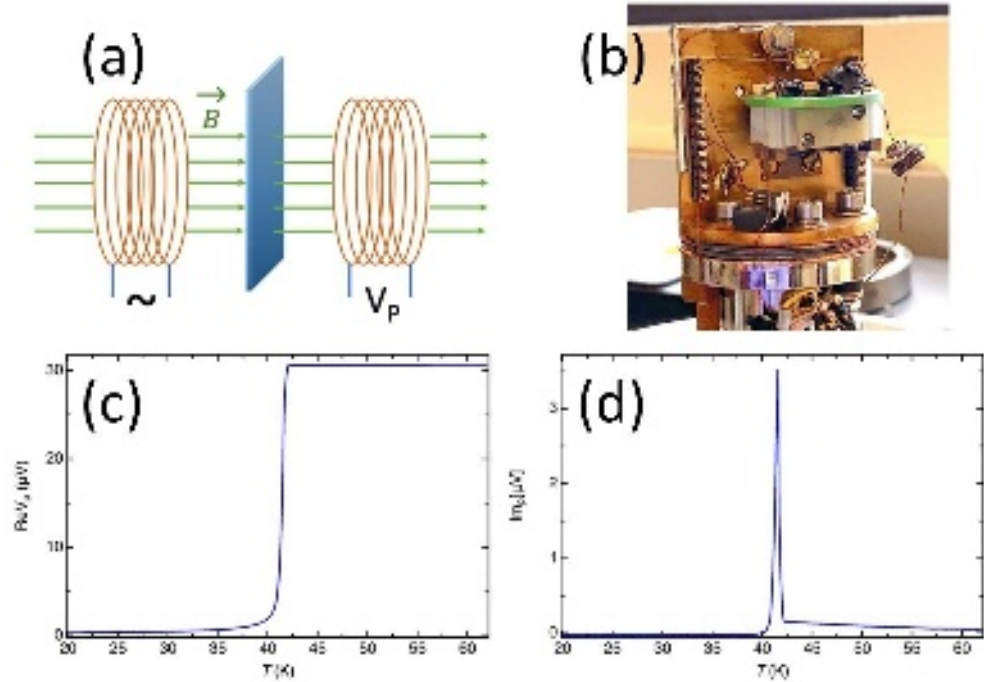


Figure 9: MI setup and data. (a) Schematic diagram of the MI measurement technique. (b) A photograph of the actual MI apparatus. (c) The real component of V_p , measured for an optimally doped LSCO film. (d) The imaginary part of V_p , for the same film.

From data such as presented in Fig. 9c and 9d, one can read T_c ; the onset of the Meissner effect (the drop in $\text{Re}V_p$) and the onset of the sharp rise in $\text{Im}V_p$ coincide with the vanishing of the resistivity in the film. We can also evaluate how homogeneous the film is. If the film had two large domains with two different values of T_c that differed by more than one half-width-at-half-maximum (HWHM), we would resolve two distinct peaks in $\text{Im}V_p$. Hence, in the LSCO film illustrated in Fig. 9c and 9d, the variations in T_c are less than 0.2 K over the $10 \times 10 \text{ mm}^2$ area.

VI. RESEARCH ENABLED BY LSCO FILMS SYNTHESIZED BY ALL-MBE

In the last two decades, using ALL-MBE we have synthesized over three thousand single-crystal LSCO thin films and characterized them extensively. The best ones have been used to study

systematically the key physical properties of LSCO, and their dependence on doping, temperature, electric and magnetic fields, irradiation, exposure to light, etc., either by ourselves or by our collaborators at many leading research institutions and universities in the USA and abroad. Together, we have made several discoveries of new phenomena. [44-66]

The insulating and the ‘normal’ metal states show unconventional behavior. (i) In a single monolayer thick film of undoped LCO, muon spin rotation experiments detect evidence of spin-liquid behavior. [44,45]. (ii) For $x < 0.06$, at very low temperature, the insulating state shows erratic switching, hysteresis, memory, etc., in both the longitudinal and Hall resistivity — the quantum-critical charge-cluster state. [46,47]. (iii) For $0.02 < x < 0.25$, the rotation symmetry is broken in the electron fluid, in the LSCO films with the tetragonal crystal structure is — the so-called electronic nematicity. [67-72] The orientation of the nematic director is reproducible, but it depends on the doping level, and it even rotates as the temperature is changed. [48] (iv) Near the optimal doping, the resistivity shows linear dependence on temperature and (in high fields) on the magnetic field strength — the so-called “strange metal” behavior. [49]. (v) Upon excitation by an ultrashort light pulse, with the electric field parallel to the CuO_2 planes, the c -axis lattice period of LSCO films increases intermittently by as much as 2-3% — the “colossal photoinduced expansion”, pointing to extremely strong electron-lattice coupling. [50]. (vi) For $0 < x < 0.30$, paramagnons are observed by resonant inelastic X-ray scattering (RIXS), with essentially the same energy but with a lifetime that shrinks with doping. [51] (vii) Fluctuating charge density waves (CDW) are observed by ultrafast intermittent-grating pump-probe spectroscopy. [52]

For the superconducting state, we have shown that it is quasi-two-dimensional (2D) by various independent, direct experiments. (viii) A single LSCO monolayer can sustain the same T_c as a bulk sample with the same doping. [53] (ix) HTS emerges at the interface of two different LCO and

heavily overdoped ($x > 0.30$) LSCO layers, neither of which would be superconducting *per se*. [54] As we have demonstrated using δ -doping tomography, this high- T_c interface superconductivity is confined to a single CuO_2 layer. [55,56] (x) The superconductor-insulator transition (SIT) occurs when the film sheet resistance exceeds the pair quantum resistance, $h/4e^2 = 6.5 \text{ K}\Omega$. (Here, h denotes the Planck constant and e the electron charge). [57].

We have also unearthed evidence of superconducting fluctuations and preformed pairs well above T_c by several independent techniques. (xi) The temperature at which phase fluctuations destroy superconductivity (the superfluid stiffness) in LSCO is low at all doping levels and comparable to T_c . More enigmatic, it decreases with doping and vanishes at the dome edge, tracking T_c . [58] At the same time, the uncondensed carrier fraction increases, even for $T \rightarrow 0$. [59] (xii) THz spectroscopy detects superconducting fluctuations up to about 20-30 K above T_c . [60] (xiii) LSCO nanorings show magnetoresistance oscillations due to the interaction of the field-shielding supercurrent with thermally excited vortices. [61] (xiv) Shot-noise measurements reveal paired charges at temperatures well above T_c and at the voltage bias up to several times the superconducting gap. [62,63]

Next, under ALL synthesis, we have been able to fabricate atomically precise multilayers and superlattices. (xv) Some of these were used to fabricate high-quality tunnel junctions, with ultrathin (down to a single unit cell thick) insulating barriers without pinholes. These can block supercurrent but revealed bosonic excitations coupled to Bogoliubov quasiparticles. [53, 62, 64] (xvi) However, when the barriers are doped to be metallic, a rather unconventional giant proximity effect is observed. [65,66]

VII. CONCLUSIONS AND OUTLOOK

In conclusion, atomically flat LSCO thin films without any secondary-phase precipitates or pinholes have been synthesized using an ALL-MBE system that was specially designed for the synthesis of HTS cuprate materials. Diagnostics based on the dynamics of RHEED image and multi-step *in-situ* post-annealing procedures have been developed to fine-tune the stoichiometry of cations and oxygen, respectively. The quality of the LSCO films is checked in real-time by RHEED and ex-situ by AFM and MI, providing fast feedback to the film grower. High-quality LSCO films have enabled fundamental studies of HTS cuprate. Furthermore, the progress in the LSCO synthesis technique has allowed us to fabricate complex heterostructures, interface superconductors, trilayer junctions, and artificial superlattices. Much of the knowledge and experience gained from LSCO synthesis is also applicable to other complex oxide compounds, so it may both aid and inspire further research of other materials and phenomena.

There is much beyond what could fit into this review. One broad topic is ALL-MBE synthesis of other cuprates, such as $\text{DyBa}_2\text{Cu}_3\text{O}_7$ (isostructural with $\text{YBa}_2\text{Cu}_3\text{O}_7$ but more amenable to MBE), various phases of $\text{Bi}_2\text{Sr}_2\text{Ca}_{n-1}\text{Cu}_n\text{O}_{2n+2}$, the so-called “infinite-layer cuprates such as $(\text{Sr,Ca})\text{CuO}_2$, etc. Another is the synthesis of complex oxides of other metals, including nickel, cobalt, ruthenium, bismuth, zinc, etc. [72-76]

A new development at Brookhaven National Laboratory is that we have completed the construction of the second ALL-MBE system, heavily customized to enable integration with *in-situ* cryogenic Angle-resolved photoemission spectroscopy (ARPES) and Spectroscopic-imaging Scanning tunneling microscopy (SI-STM) systems. This complex new three-in-one facility makes it possible to synthesize state-of-the-art films of various cuprates and other complex oxides by ALL-MBE and transfer them without breaking the ultra-high vacuum to ARPES and/or SI-STM modules for determination of the electronic spectrum, with high spatial and momentum resolution. This

eliminates the need to cleave the samples and thus greatly broadens the spectrum of materials amenable to study by these surface-sensitive techniques. [77,78]

ACKNOWLEDGMENTS

This research was done at BNL and was supported by the U.S. Department of Energy, Basic Energy Sciences, Materials Sciences and Engineering Division. H.X. is supported by the Gordon and Betty Moore Foundation's EPIQS Initiative through Grant GBMF9074.

AUTHOR DECLARATIONS

The authors declare no competing financial interests.

DATA AVAILABILITY

The data that support the findings of this study are available from the corresponding author upon reasonable request, addressed to bozovic@bnl.gov.

REFERENCES

1. J. G. Bednorz and K. A. Müller, "Possible high T_c superconductivity in the Ba-La-Cu-O system", *Z. Physik B - Condensed Matter* 64, 189-193 (1986). doi.org/10.1007/BF01303701
2. P. W. Anderson, "The resonating valence bond state in La_2CuO_4 and superconductivity", *Science* 235, 1196-1198 (1987). doi.org/10.1126/science.235.4793.1196
3. V. Emery and S. A. Kivelson, "Importance of phase fluctuations in superconductors with small superfluid density", *Nature* 374, 434-437 (1994). doi.org/10.1038/374434a0
4. A. S. Alexandrov and N. F. Mott, *High Temperature Superconductors and Other Superfluids* (Taylor and Francis, 1994).

5. G. M. Zhao, M. B. Hunt, H. Keller and K. A. Muller, “Evidence for polaronic supercarriers in the copper oxide superconductors $\text{La}_{2-x}\text{Sr}_x\text{CuO}_4$ ”, *Nature* 381, 676-678 (1996).
doi.org/10.1038/385236a0
6. P. W. Anderson, *The theory of superconductivity in the high- T_c cuprates* (Princeton University Press, 1997).
7. H. Sato, A. Tsukada, M. Naito and A. Matsuda, “ $\text{La}_{2-x}\text{Sr}_x\text{CuO}_y$ epitaxial films ($x = 0$ to 2): Structure, strain, and superconductivity”, *Phys. Rev. B* 61, 12447 (2000).
doi.org/10.1103/PhysRevB.61.12447
8. I. Bozovic, G. Logvenov, M. A. J. Verhoeven, P. Caputo, E. Goldobin and T. H. Geballe, “No mixing of superconductivity and antiferromagnetism in a high temperature superconductor”, *Nature* 422, 873-875 (2003). doi.org/10.1038/nature01544
9. A. Damascelli, Z. Hussain and Z. X. Shen, “Angle-resolved photoemission studies of the cuprate superconductors”, *Rev. Mod. Phys.* 75, 473-541 (2003).
doi.org/10.1103/RevModPhys.75.473
10. J. Zaanen, “Superconductivity: Why the temperature is high”, *Nature* 430, 512-513 (2004).
doi.org/10.1038/430512a
11. Q. J. Chen, J. Stajic, S. Tan and K. Levin, “BCS-BEC crossover: From high temperature superconductors to ultracold superfluids”, *Physics Reports* 412, 1-88 (2005).
doi.org/10.1016/j.physrep.2005.02.005
12. V. Z. Kresin, Y. N. Ovchinnikov and S. A. Wolf, “Inhomogeneous superconductivity and the “pseudogap” state of novel superconductors”, *Physics Reports* 431, 231-259, (2006).
doi.org/10.1016/j.physrep.2006.05.006

13. J. Zaanen, S. Chakravarty, T. Senthil, P. W. Anderson, P. Lee, J. Schmalian, M. Imada, D. Pines, M. Randeria, C. Varma, M. Vojta and M. Rice, “Towards a complete theory of high T_c ”, *Nature Phys.* 2, 138-143 (2006). doi.org/10.1038/nphys253
14. Q. Chen, K. Levin and J. Stajic, “Applying BCS-BEC crossover theory to high-temperature superconductors and ultracold atomic Fermi gases”, *Low Temp. Phys.* 32, 406-423 (2006). doi.org/10.1063/1.2199443
15. P. A. Lee, N. Nagaosa and X. G. Wen, “Doping a Mott insulator: Physics of high-temperature superconductivity”, *Rev. Mod. Phys.* 78,17 (2006). doi.org/10.1103/RevModPhys.78.17
16. R. B. Laughlin, “Fermi-Liquid Computation of the Phase Diagram of High- T_c Cuprate Superconductors with an Orbital Antiferromagnetic Pseudogap”, *Phys. Rev. Lett.* 112, 017004 (2014). doi.org/10.1103/PhysRevLett.112.017004
17. R. B. Laughlin, “Hartree-Fock computation of the high- T_c cuprate phase diagram”, *Phys. Rev. B* 89, 035134 (2014). doi.org/10.1103/PhysRevB.89.035134
18. P. A. Lee, “Amperean Pairing and the Pseudogap Phase of Cuprate Superconductors”, *Phys. Rev. X* 4, 031017 (2014). doi.org/10.1103/PhysRevX.4.031017
19. B. Keimer, S. A. Kivelson, M. R. Norman, S. Uchida and J. Zaanen. “From quantum matter to high-temperature superconductivity in copper oxides”, *Nature* 518, 179-186 (2015). doi.org/10.1038/nature14165
20. J. Zaanen, “Superconducting electrons go missing”, *Nature* 536, 282-283 (2016). doi.org/10.1038/536282a
21. I. Božović, J. Wu, X. He and A. T. Bollinger, “What is really extraordinary in cuprate superconductors?”, *Physica C* 558, 30-37 (2019). doi.org/10.1016/j.physc.2018.02.055

22. J. N. Eckstein and I. Bozovic, "High-temperature superconducting multilayers and heterostructures grown by atomic layer-by-layer molecular beam epitaxy", *Annual Reviews of Materials Science* 25, 679-709 (1995). doi.org/10.1146/annurev.ms.25.080195.003335
23. I. Bozovic, "Atomic-layer engineering of superconducting oxides: Yesterday, today, tomorrow", *IEEE Trans Appl Supercond.* 11, 2686-2695 (2001). doi.org/10.1109/77.919617
24. M. Naito and H. Sato, "Stoichiometry control of atomic beam fluxes by precipitated impurity phase detection in growth of (Pr,Ce)₂CuO₄ and (La,Sr)₂CuO₄ films", *Appl. Phys. Lett.* 67, 2557 (1995). doi.org/10.1063/1.114431
25. M. Naito, H. Sato and H. Yamamoto, "MBE growth of (La,Sr)₂CuO₄ and (Nd,Ce)₂CuO₄ thin films", *Physica C* 293, 36-43 (1997). doi.org/10.1016/S0921-4534(97)01510-4
26. J.-P. Locquet, J. Perret, J. Fompeyrine, E. Machler, J. W. Seo, and G. Van Tendeloo, "Doubling the critical temperature of La_{1.9}Sr_{0.1}CuO₄ using epitaxial strain", *Nature* 394, 453-456 (1998). doi.org/10.1038/28810
27. H. Sato, A. Tsukada, M. Naito, and A. Matsuda, "La_{2-x}Sr_xCuO_y epitaxial thin films (x = 0 to 2): Structure, strain, and superconductivity", *Phys. Rev. B* 61, 12447 (2000). doi.org/10.1103/PhysRevB.61.12447
28. A. Biswas, P. B. Rossen, J. Ravichandran, Y.-H. Chu, Y.-W. Lee, C.-H. Yang, R. Ramesh and Y. H. Jeong, "Selective A- or B-site single termination on surfaces of layered oxide SrLaAlO₄", *Appl. Phys. Lett.* 102, 051603 (2013). doi.org/10.1063/1.4790575
29. M. Kawasaki, K. Takahashi, T. Maeda, R. Tsuchiya, M. Shinohara, O. Ishiyama, T. Yonezawa, M. Yoshimoto, and H. Koinuma, "Atomic Control of the SrTiO₃ Crystal Surface", *Science* 266, 1540-1542 (1994). doi.org/10.1126/science.266.5190.1540

30. A. Biswas, P. B. Rossen, C.-H. Yang, W. Siemons, M.-H. Jung, I. K. Yang, R. Ramesh and Y. H. Jeong, “Universal Ti-rich termination of atomically flat SrTiO₃ (001), (110), and (111) surfaces”, Appl. Phys. Lett. 98, (2011). doi.org/10.1063/1.3549860
31. J. G. Connell, B. J. Isaac, G. B. Ekanayake, D. R. Strachan and S. S. A. Seo, “Preparation of atomically flat SrTiO₃ surfaces using a deionized-water leaching and thermal annealing procedure”, Appl. Phys. Lett. 101, 98-101 (2012). doi.org/10.1063/1.4773052
32. M. Jager, A. Teker, J. Mannhart and W. Braun, “Independence of surface morphology and reconstruction during the thermal preparation of perovskite oxide surfaces”, Appl. Phys. Lett. 112, 111601 (2018). doi.org/10.1063/1.5023318
33. W. Braun, M. Jager, G. Laskin, P. Ngabonziza, W. Voesch, P. Wittlich and J. Mannhart, “In situ thermal preparation of oxide surfaces”, APL Materials 8, 071112 (2020). doi.org/10.1063/5.0008324
34. M. Naito, H. Yamamoto, H. Sato, “Intrinsic problem of cuprate surface and interface: why good tunnel junctions are difficult to fabricate”, Physica C 335, 201-206 (2000). doi.org/10.1016/S0921-4534(00)00171-4
35. N. Nakagawa, H. Y. Hwang and D. A. Muller, “Why some interfaces cannot be sharp”, Nat. Mater. 5, 204–209 (2006). doi.org/10.1038/nmat1569
36. R. Pentcheva and W. E. Pickett, “Avoiding the polarization catastrophe in LaAlO₃ overlayers on SrTiO₃ (001) through polar distortion”, Phys. Rev. Lett. 102, 107602 (2009). doi.org/10.1103/PhysRevLett.102.107602
37. I. Bozovic and J. N. Eckstein, “Analysis of Growing Films of Complex Oxides by RHEED”, MRS Bull. 20, 32-38 (1995). doi.org/10.1557/S0883769400044870

This is the author's peer reviewed, accepted manuscript. However, the online version of record will be different from this version once it has been copyedited and typeset.
PLEASE CITE THIS ARTICLE AS DOI:10.1063/5.0087223

38. Note that this is true for 99%, or more, of the HTS films grown by any technique. So far, just a handful of groups around the globe have demonstrated the capability to grow single-phase, single-crystal HTS films without any secondary-phase precipitates.
39. I. Bozovic, G. Logvenov, I. Belca, B. Narimbetov and I. Sveklo, “Epitaxial Strain and Superconductivity in $\text{La}_{2-x}\text{Sr}_x\text{CuO}_4$ Thin Films”, *Phys. Rev. Lett.* 89, 107001 (2002).
doi.org/10.1103/PhysRevLett.89.107001
40. P. G. Radaelli, D. G. Hinks, A. W. Mitchell, B.A. Hunter, J. L. Wagner, B. Dabrowski, K. G. Vandervoort, H. K. Viswanathan, and J. D. Jorgensen, “Structural and superconducting properties of $\text{La}_{2-x}\text{Sr}_x\text{CuO}_4$ as a function of Sr content”, *Phys. Rev. B* 49, 4163-4175 (1994).
doi.org/10.1103/PhysRevB.49.4163
41. X. Leng and I. Božović, “Controlling Superconductivity in $\text{La}_{2-x}\text{Sr}_x\text{CuO}_{4+\delta}$ by Ozone and Vacuum Annealing”, *J. Supercond. Nov. Magn.* 28, 71-74 (2015). doi.org/10.1007/s10948-014-2888-2
42. R. H. Hammond and R. Bormann, “Correlation between the in situ growth conditions of YBCO thin films and the thermodynamic stability criteria”, *Physica. C* 162-164, 703-704 (1989).
[doi.org/10.1016/0921-4534\(89\)91218-5](https://doi.org/10.1016/0921-4534(89)91218-5)
43. X. He, A. Gozar, R. Sundling and I. Božović, “High-precision measurement of magnetic penetration depth in superconducting films”, *Rev. Sci. Instrum.* 87, 113903 (2016).
doi.org/10.1063/1.4967004
44. A. Suter, E. Morenzoni, T. Prokscha, B. M. Wojek, H. Luetkens, G. Nieuwenhuys, A. Gozar, G. Logvenov and I. Bozovic, “Two-Dimensional Magnetic and Superconducting Phases in Metal-Insulator $\text{La}_{2-x}\text{Sr}_x\text{CuO}_4$ Superlattices Measured by Muon-Spin Rotation”, *Phys. Rev. Lett.* 106, 237003 (2011). doi.org/10.1103/PhysRevLett.106.237003

45. M. P. M. Dean, R. S. Springell, C. Monney, K. J. Zhou, I. Bozovic, J. Pereiro, B. Dalla Piazza, H. M. Ronow, J. van den Brink, T. Schmitt and J. P. Hill, “Spin Excitations in a single La_2CuO_4 layer”, *Nature Materials* 11, 850-854 (2012). doi.org/10.1038/nmat3409
46. X. Shi, D. Popović, C. Panagopoulos, G. Logvenov, A. T. Bollinger and I. Bozovic, “Emergence of superconductivity from the dynamically heterogeneous insulating state in $\text{La}_{2-x}\text{Sr}_x\text{CuO}_4$ ”, *Nature Materials* 12, 47-51 (2013). doi.org/10.1038/nmat3487
47. J. Wu, A. T. Bollinger, Y.-J. Sun and I. Božović, “Hall Effect in quantum critical charge-cluster glass”, *Proc. Natl. Acad. Sci. USA (PNAS)* 113, 4284-4829 (2016). doi.org/10.1073/pnas.1519630113
48. J. Wu, A. T. Bollinger, X. He and I. Božović, “Spontaneous breaking of rotational symmetry in copper oxide superconductors”, *Nature* 547, 432-436 (2017). doi.org/10.1038/nature23290
49. P. Giraldo-Gallo, J. A. Galvis, Z. Stegen, K. A. Modic, F. F Balakirev, J. B. Betts, X.-J. Lian, C. Moir, S. C. Riggs, J. Wu, A. T. Bollinger, X. He, I. Bozovic, B. J. Ramshaw, R. D. McDonald, G. S. Boebinger and A. Shekhter, “Scale invariant magnetoresistance in the strange metal phase of a cuprate superconductor”, *Science* 361, 479-481 (2018). doi.org/10.1126/science.aan3178
50. N. Gedik, D.-S. Yang, G. Logvenov, I. Bozovic and A. Zewail, “Non-equilibrium Phase Transitions in Cuprates Observed by Ultrafast Electron Crystallography.” *Science* 316, 425-429 (2007). doi.org/10.1126/science.1138834
51. M. P. M. Dean, G. Dellea, R. S. Springell, F. Yakhou-Harris, K. Kummer, N. B. Brookes, X. Liu, Y.-J. Sun, J. Strle, T. Schmitt, L. Braicovich, G. Ghiringhelli, I. Bozovic and J. P. Hill, “Persistence of magnetic excitations in $\text{La}_{2-x}\text{Sr}_x\text{CuO}_4$ from the undoped insulator to the

- heavily overdoped non-superconducting metal”, *Nature Materials* 12, 1019-1023 (2013).
doi.org/10.1038/nmat3723
52. D. H. Torchinsky, F. Mahmood, A. T. Bollinger, I. Božović and N. Gedik, “Fluctuating charge density waves in a cuprate superconductor”, *Nature Materials* 12, 387-391 (2013).
doi.org/10.1038/nmat3571
53. I. Bozovic, G. Logvenov, M. A. J. Verhoeven, P. Caputo, E. Goldobin and T. H. Geballe, “No mixing of superconductivity and anti-ferromagnetism in a high-critical-temperature superconductor”, *Nature* 422, 873-875 (2003). doi.org/10.1038/nature01544
54. A. Gozar, G. Logvenov, L. Fitting Kourkoutis, A. T. Bollinger, L. A. Giannuzzi, D. A. Muller, and I. Bozovic, “High-temperature Interface superconductivity between a metal and a Mott insulator”, *Nature* 455, 782-785 (2008). doi.org/10.1038/nature07293
55. G. Logvenov, A. Gozar and I. Bozovic, “High-temperature superconductivity in a single copper-oxygen plane”, *Science* 326, 699-702 (2009). doi.org/10.1126/science.1178863
56. J. Wu, O. Pelleg, G. Logvenov, A. T. Bollinger, Y. Sun, G. S. Boebinger, M. Vanević, Z. Radović and I. Božović, “Anomalous independence of interface superconductivity on carrier density”, *Nature Materials* 12, 877-881 (2013). doi.org/10.1038/nmat3719
57. A. T. Bollinger, G. Dubuis, J. Yoon, D. Pavuna, J. Misewich and I. Bozovic, “Superconductor–insulator transition in $\text{La}_{2-x}\text{Sr}_x\text{CuO}_4$ at the pair quantum resistance”, *Nature* 472, 458-460 (2011). doi.org/10.1038/nature09998
58. I. Božović, J. Wu, X. He and A. T. Bollinger, “Dependence of critical temperature in overdoped copper oxides on superfluid density”, *Nature* 536, 309-311 (2016).
doi.org/10.1038/nature19061

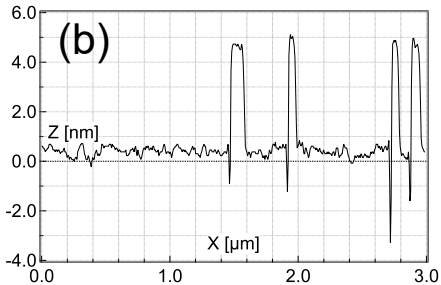
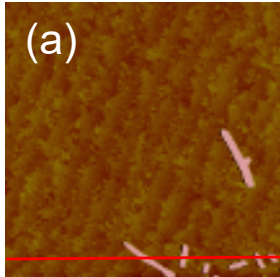
59. F. Mahmood, X. He, I. Božović and N. P. Armitage, “Locating the missing superconducting electrons in overdoped cuprates”, *Phys. Rev. Lett.* 122, 027003 (2019).
doi.org/10.1103/PhysRevLett.122.027003
60. L. S. Bilbro, R. Valdés Aguilar, G. Logvenov, O. Pelleg, I. Bozovic and N. P. Armitage, “Temporal correlations of superconductivity above the transition temperature in $\text{La}_{2-x}\text{Sr}_x\text{CuO}_4$ probed by terahertz spectroscopy”, *Nature Physics* 7, 298-302 (2011).
doi.org/10.1038/nphys1912
61. I. Sochnikov, A. Shaulov, Y. Yeshurun, G. Logvenov and I. Bozovic, “Large oscillations of the magnetoresistance in nanopatterned high-temperature superconducting films”, *Nature Nanotechnology* 5, 516-519 (2010). doi.org/10.1038/nnano.2010.111
62. P. Zhou, L. Chen, Y. Liu, I. Sochnikov, A. T. Bollinger, M.-G. Han, Y. Zhu, X. He, I. Božović and D. Natelson, “Electron pairing in the pseudogap state revealed by shot noise in copper-oxide junctions”, *Nature* 572, 493-496 (2019). doi.org/10.1038/s41586-019-1486-7
63. I. Božović and J. Levy, “Pre-Formed Pairs in Copper Oxides and $\text{LaAlO}_3/\text{SrTiO}_3$ ”, *Nature Physics* 16, 712-717 (2020). doi.org/10.1038/s41567-020-0915-8
64. P. Zhou, L. Chen, I. Sochnikov, T. C. Wu, M. S. Foster, A. T. Bollinger, X. He, I. Božović and D. Natelson, “Tunneling spectroscopy of c-axis epitaxial cuprate junctions”, *Phys. Rev. B* 101, 224512 (2020). doi.org/10.1103/PhysRevB.101.224512
65. I. Bozovic, G. Logvenov, M. A. J. Verhoeven, P. Caputo, E. Goldobin and M. R. Beasley, “Giant Proximity Effect in cuprate superconductors”, *Phys. Rev. Lett.* 93, 157002 (2004).
doi.org/10.1103/PhysRevLett.93.157002

66. E. Morenzoni, B. M. Wojek, A. Suter, T. Prokscha, G. Logvenov and I. Bozovic, “The Meissner effect in a strongly underdoped cuprate above its critical temperature”, *Nature Communications* 2, 272 (2011). doi.org/10.1038/ncomms1273
67. J. Zaanen and O. Gunnarsson, “Charged magnetic domain lines and the magnetism of high- T_c oxides”, *Phys. Rev. B* 40, 7391-7394 (1989). doi.org/10.1103/PhysRevB.40.7391
68. J. Zaanen and A. M. Oles, “Striped phase in the cuprates as a semiclassical phenomenon”, *Annalen der Physik* 5, 224-246 (1996). doi.org/10.1002/andp.2065080303
69. S. A. Kivelson, E. Fradkin and V. J. Emery, “Electronic liquid-crystal phases of a doped Mott insulator”, *Nature* 393, 550-553 (1998). doi.org/10.1038/31177
70. V. Oganesyan, S. A. Kivelson and E. Fradkin, “Quantum theory of a nematic Fermi fluid”, *Phys. Rev. B* 64, 195109 (2001). doi.org/10.1103/PhysRevB.64.195109
71. E. Fradkin, S. A. Kivelson, M. J. Lawler, J. P. Eisenstein and A. P. Mackenzie, “Nematic Fermi fluids in condensed matter physics”, *Ann. Rev. Cond. Mat. Phys.* 1, 153-178 (2010). doi.org/10.1146/annurev-conmatphys-070909-103925
72. I. Bozovic, J. H. Kim, J. S. Harris Jr., J. Cheung and C. B. Eom, “Reflectance and Raman Spectra of Metallic Oxides, La-Sr-Co-O and Sr-Ca-Ru-O: Resemblance to Superconducting Cuprates”, *Phys. Rev. Lett.* 73, 1436-1439 (1994). doi.org/10.1103/PhysRevLett.73.1436
73. D. Kirillov, Y. Suzuki, L. Antognazza, K. Char, I. Bozovic and T. H. Geballe, “Phonon anomalies at the magnetic phase transitions in SrRuO_3 ”, *Phys. Rev. B* 51, 12825-12828 (1995). doi.org/10.1103/PhysRevB.51.12825
74. A. Gozar, G. Logvenov, V. Butko and I. Bozovic, “Surface structure analysis of atomically smooth BaBiO_3 films”, *Phys. Rev. B* 75, 201402 (2007). doi.org/10.1103/PhysRevB.75.201402

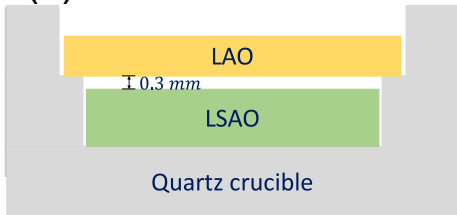
This is the author's peer reviewed, accepted manuscript. However, the online version of record will be different from this version once it has been copyedited and typeset.
PLEASE CITE THIS ARTICLE AS DOI:10.1063/5.0087223

75. P. D. C. King, H. I. Wei, Y. F. Nie, M. Uchida, C. Adamo, S. Zhu, X. He, I. Bozovic, D. G. Schlom and K. M. Shen, “Atomic-scale control of competing electronic phases in ultrathin LaNiO_3 ”, *Nature Nanotechnology* 9, 443-447 (2014). doi.org/10.1038/nnano.2014.59
76. C. K. Kim, I. Drozdov, K. Fujita, J. C. Davis, I. Božović and T. Valla, “In-situ angle-resolved photoemission spectroscopy of copper-oxide thin films synthesized by molecular beam epitaxy”, *Journal of Electron Spectroscopy and Related Phenomena* (2018)
doi.org/10.1016/j.elspec.2018.07.003
77. J. Wu, H. P. Nair, A. T. Bollinger, X. He, I. Robinson, J. P. Ruf, N. J. Schreiber, K. M. Shen, D. G. Schlom and I. Božović, “Electronic nematicity in Sr_2RuO_4 ”, *PNAS* 117, 10654-10659 (2020). doi.org/10.1073/pnas.1921713117
78. H. Li, Z. Du, Z. Wu, D. Putzky, S. H. Joo, A. K. Kundu, X. Xu, X. Shi, J. Lee, A. N. Pasupathy, G. Logvenov, B. Keimer, T. Valla, I. Božović, I. K. Drozdov and K. Fujita, “Visualizing the unusual spectral weight transfer in $\text{DyBa}_2\text{Cu}_3\text{O}_{7-\delta}$ thin film”, *Scientific Reports* 12, 830 (2022). doi.org/10.1038/s41598-021-04692-9

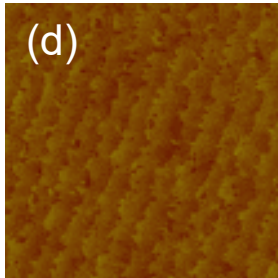
(a)

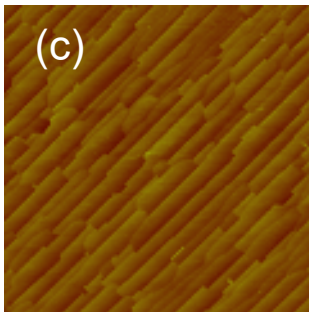
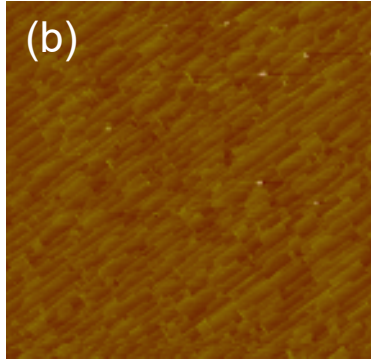
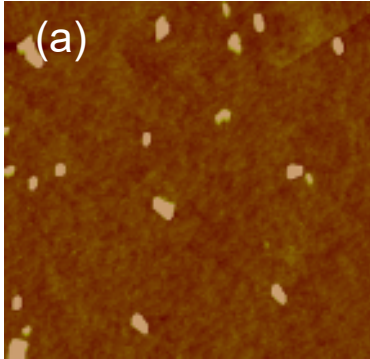


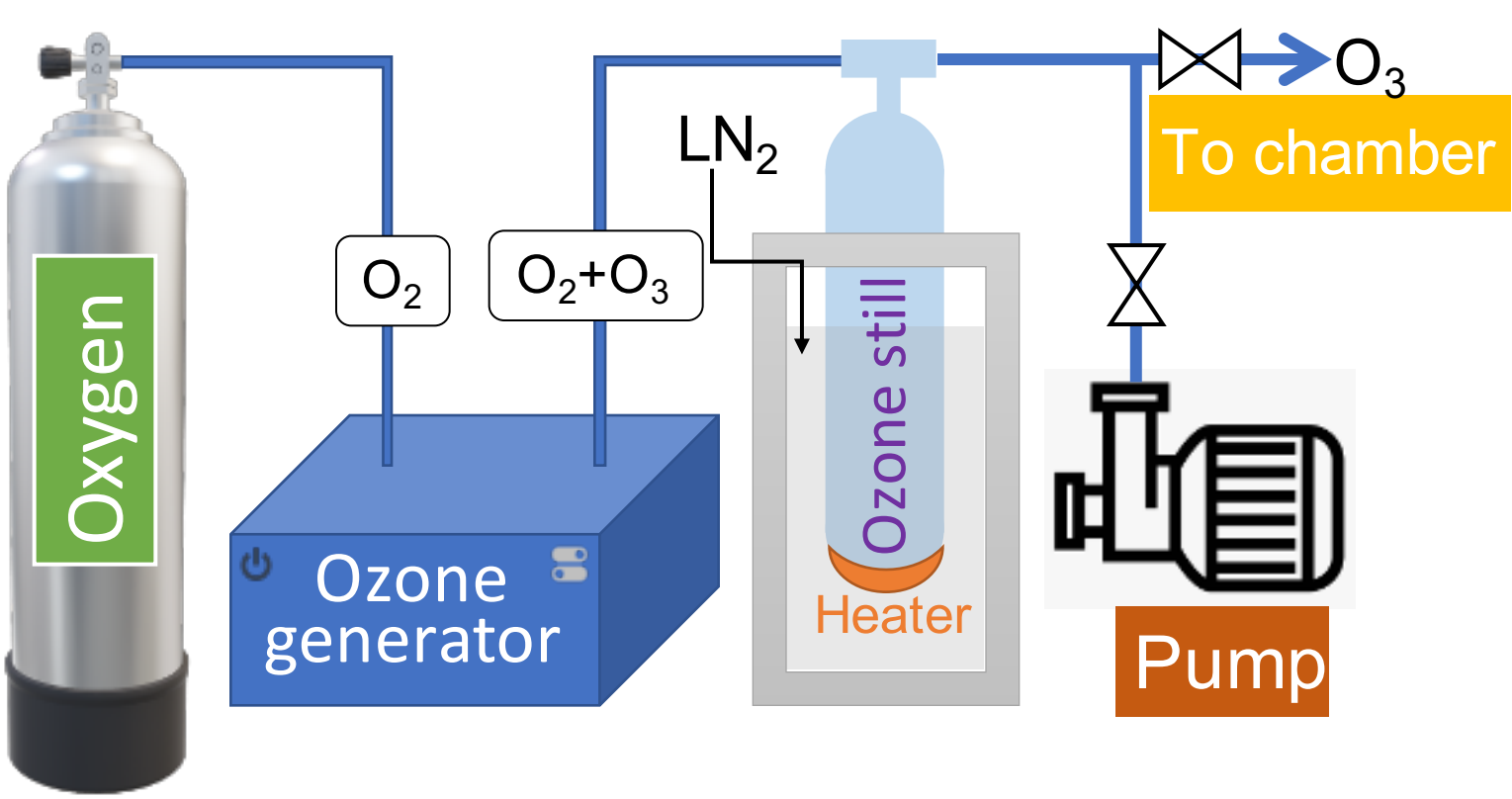
(c)

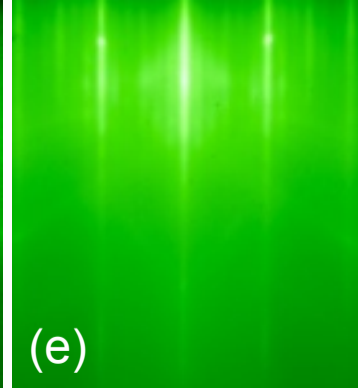
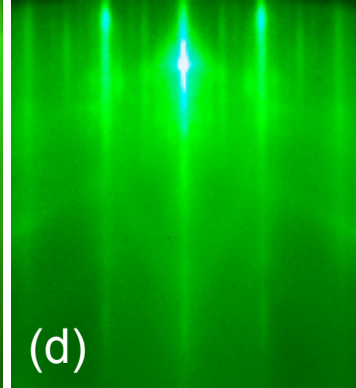
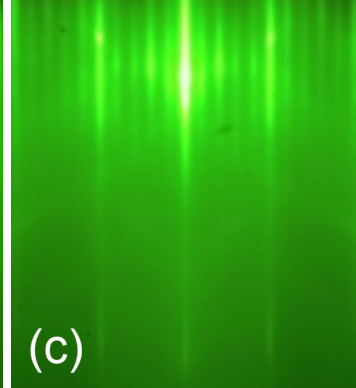
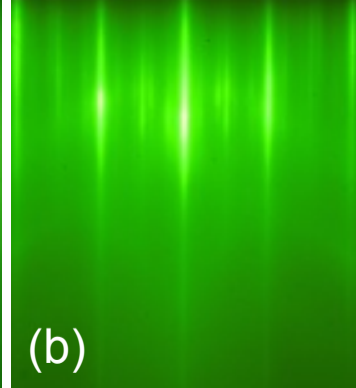
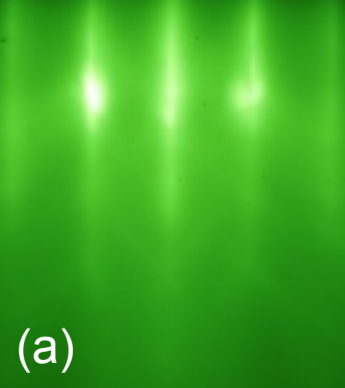


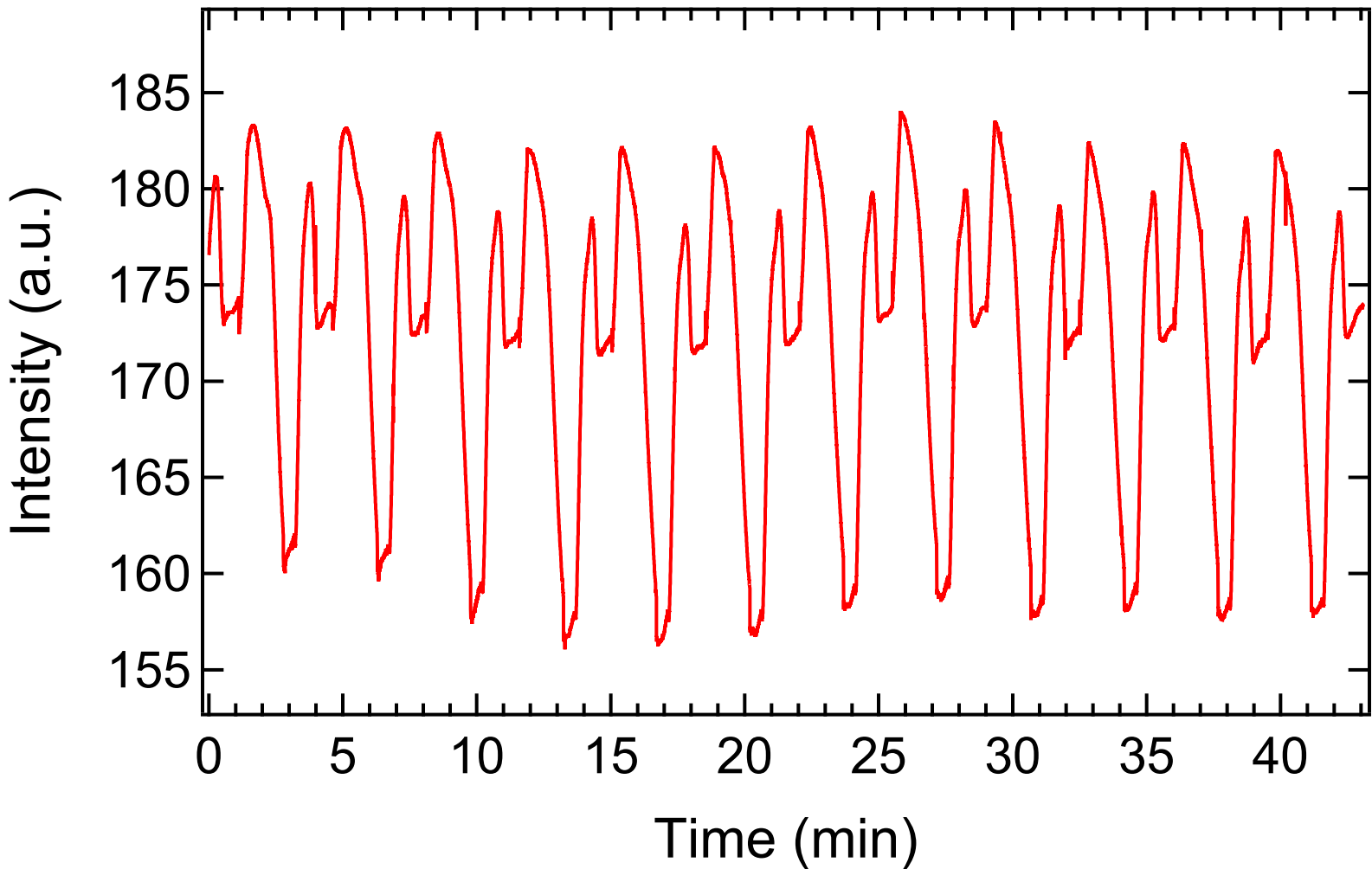
(d)



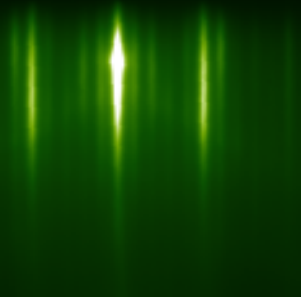




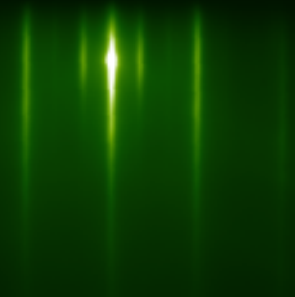


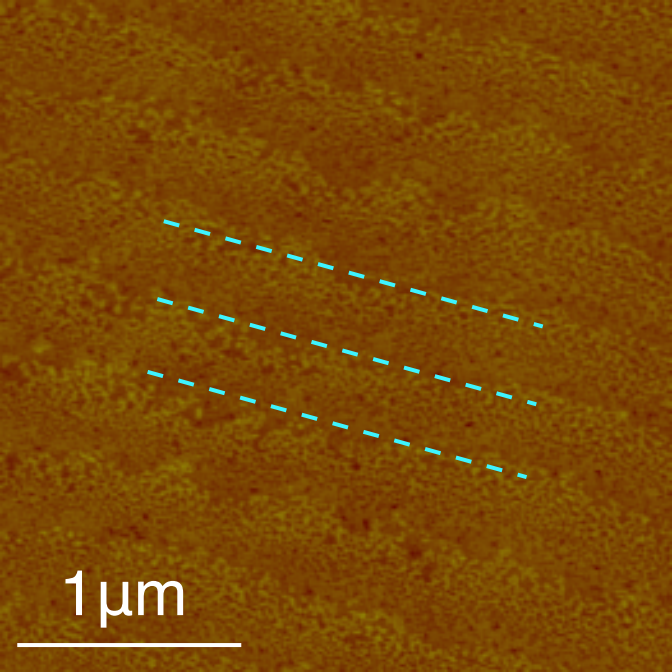


(a)



(b)





1 μm

